Separation and Purification Technology 324 (2023) 124489

Contents lists available at ScienceDirect

Separation and Purification Technology

journal homepage: www.elsevier.com/locate/seppur

Development of high capacity moisture-swing DAC sorbent for direct air capture of CO_2

Xueru Wang [a,b], Yan Chen [a], Wenqi Xu [b], Arne Lindbråthen [b], Xinyue Cheng [c], Xi Chen [d], Liangliang Zhu [c,*], Liyuan Deng [b,*]

[a] Laboratory for Multiscale Mechanics and Medical Science, SV LAB, School of Aerospace, Xi'an Jiaotong University, Xi'an 710049, China
[b] Department of Chemical Engineering, Norwegian University of Science and Technology, Trondheim 7491, Norway
[c] School of Chemical Engineering, Northwest University, Xi'an 710069, China
[d] Department of Earth and Environmental Engineering, Columbia University, New York, NY 10027, USA

ARTICLE INFO

Keywords:
Moisture-swing sorbents
Anion-exchange resin
Direct air capture
CO_2 ad-/desorption
Quaternary ammonium

ABSTRACT

Direct air capture (DAC) of CO_2 complements traditional carbon capture technologies to achieve zero- or negative-carbon emissions. One of the most promising DAC technologies is moisture-swing adsorption due to its low regeneration costs and easiness of operation, particularly when using amine-based anion-exchange resins (AER) as sorbents, but the limited CO_2 sorption capacity and desorption efficiency of current AERs are still critical challenges hindering the large-scale implementation of DAC. For the first time, this work developed a novel diamine-based double quaternary ammonium anion-exchange resins (Diamine-DQ-AER) by modifying commercial resins with tertiary diamines. The significantly improved quaternary ammonium content in Diamine-DQ-AER (68–81 %) compared to diamine-based single quaternary ammonium anion-exchange resins (Diamine-SQ-AER) resulted in an unprecedented moisture-swing DAC capacity of 3.41 mmol/g under DAC conditions, nearly doubled that of Diamine-SQ-AER. Diamine-DQ-AER also showed a stable capacity in the 6-cycle test, outperforming most moisture-swing DAC sorbents reported in the literature. Moreover, a complete desorption kinetic curve was obtained using an optimized testing protocol. It found that the CO_2 adsorption/desorption process involves two stages, and the material exhibited fast desorption kinetics in the 1st stage.

1. Introduction

The use of fossil fuels for power generation and the consequent emission of a large amount of carbon dioxide into the atmosphere is considered the primary cause of global warming, today's major challenge for humankind [1]. The summary for policymakers of the IPCC Sixth Assessment Report (AR6) [2] has reaffirmed that the global surface temperature will continue to increase unless deep reduction actions are taken worldwide. Carbon capture, utilization, and storage technologies (CCUS) have been implemented globally as the immediate solution to mitigate climate change [3,4], which are, however, currently concentrating primarily on large point-source capture of CO_2 and use mostly traditional absorption or adsorption technologies that require high regeneration energy input with unavoidable solvent loss, amine volatilization, and are limited by locations [5,6].

Direct air capture (DAC), capturing CO_2 directly from ambient air, is an emerging technology with the potential to deal with distributed and mobile carbon emission sources and compensate for the escaped and residual emissions outside of the centralized large point-source capture processes without being restricted by storage sites and CO_2 transportation [7,8]. DAC has now been considered a promising approach and a necessary complement to traditional CCUS pathways. A wide range of sorbent materials for DAC has been extensively studied [9,10]. The CO_2 adsorption capacity of physisorption materials (such as MOFs and zeolite) is usually in the range of 0.02–1.3 mmol/g [11-14], but the sorption competition and reaction with atmospheric moisture significantly reduced their DAC performance. Strong alkaline materials, including metal hydroxides or oxides [15,16] and alkaline salts [17,18], can easily absorb CO_2 from the air and convert it to metal carbonates via chemisorption with a capacity of 4.5 mmol/g (CaO) and 11 mmol/g ($Ca(OH)_2$) [19]. However, releasing CO_2 requires heating the material to high temperatures, which makes DAC using strong alkaline materials technically and economically challenging. Amine-modified sorbents, exhibiting CO_2 adsorption capacity under DAC conditions in the range of

* Corresponding author.
E-mail addresses: zhu.liangliang@nwu.edu.cn (L. Zhu), liyuan.deng@ntnu.no (L. Deng).

https://doi.org/10.1016/j.seppur.2023.124489
Received 1 June 2023; Received in revised form 30 June 2023; Accepted 30 June 2023
Available online 7 July 2023

0.17–6.85 mmol/g [20-23], but their regeneration is also energy-intensive even though they have long been practiced in commercial-scale CO_2 separation from flue gas. Other materials such as amino acid and guanidine compound sorbents [24-27], electrochemical/PH swing CO_2 sorbents [28-31], and moisture swing CO_2 sorbents [32-39] are emerging in the field of DAC with the highest CO_2 adsorption capacity reported to be 1.61 mmol/g [26], 1.76 mmol/g [31] and 1.02 mmol/g [40], respectively. Nevertheless, the adsorption performance, influencing factors, material stability, testing, and application of these DAC sorbents still require extensive research and optimization before they can be commercialized for DAC applications.

Among the reported DAC sorbents, the moisture-swing direct air capture sorbents (MSDACS) have shown great potential to capture CO_2 with low costs[9,15,16]. The MSDACS is usually functionalized with ammonium groups ($-N^+(CH_3)_3$) and carbonate ions (CO_3^{2-}). Based on the water-driven reversible reaction mechanism, as shown in Eq. (1), the MSDACS can absorb CO_2 spontaneously from ambient air when it is dry and release CO_2 when it is wet [33]. The moisture-swing process between adsorption and desorption is triggered by the change of humidity instead of changing temperature or pressure.

$$2\left[\text{-}N^+(CH_3)_3\right]\text{-}CO_3^{2-}\cdot nH_2O \leftrightarrow [\text{-}N^+(CH_3)_3]\text{-}HCO_3^-\cdot m_1H_2O + [\text{-}N^+(CH_3)_3]\text{-}OH^-\cdot m_2H_2O + (n\text{-}m_1\text{-}m_2\text{-}1)H_2O \quad (1)$$

Researchers have developed a series of MSDACS, among which the amine-based AER has become the most studied because of its stable chemical structure and good ion exchange capacity [34-37]. In addition to AER, other functional porous materials [41], such as modified carbon black [42], colloidal crystals [43], high internal phase emulsion (HIPE) polymers [44], mesoporous polymers [45], and inexpensive biomass materials, such as quaternized cellulose [38] and chitosan/PVA aerogels [39], have greatly extended the family of MSDACS. However, the CO_2 ad-/desorption capacity of the above MSDACS is only 0.1–1.02 mmol/g [40,41], which is far less than that of other DAC sorbents. Thus, low CO_2 sorption capacity in MSDACS has become the main bottleneck for the implementation of moisture swing technology in commercial applications.

In this work, tertiary diamines were introduced to a commercial resin (Merrifield resin) to enhance the DAC capacity of the amine-based anion-exchange resins (AER) and develop novel diamine-based double quaternary ammonium AER (Diamine-DQ-AER). Thanks to the improved content of quaternary ammonium, the as-prepared Diamine-DQ-AER exhibited superior DAC performance of ~3.41 mmol/g as moisture-swing CO_2 sorbents at room temperature and atmospheric conditions, which is ~1.94 times that of diamine-based single quaternary ammonium AER (Diamine-SQ-AER). Moreover, Diamine-DQ-AERs showed stable DAC capacity in the 6-cycle tests. We have also optimized the test method to measure the complete desorption kinetic curve, revealing a two-stage desorption process, and the material displayed fast desorption kinetics in the first stage.

2. Materials and methods

2.1. Material

Divinylbenzene-crosslinked chloromethyl polystyrene (Merrifield resin with different chlorine content) was purchased from Tianjin Nankai Hecheng Science & Technology Co. Ltd., China. IRA-900 resins were purchased from Rohm and Haas, Inc., American. Diamines, including N,N,N'N'-tetramethylethylenediamine (TEMED), 1,4-dimethylpiperazine (DMP), and 1,4-diazabicyclo[2,2,2]octane (DABCO), were purchased from Sigma-Aldrich, Norway. Iodomethane (CH_3I), tetrabutylammonium bromide, N,N-Dimethylformamide (DMF), hydrochloric acid solution (HCl 37 % wt.%), sodium hydroxide (NaOH), sodium chloride (NaCl), and sodium carbonate (Na_2CO_3) were also purchased from Sigma-Aldrich, Norway. All chemicals were used as-received without further purification. The chemical structures of the key chemicals are depicted in Fig. 1.

2.2. Preparation of Diamine-SQ/DQ-AER

2.2.1. Preprocessing of Merrifield resin

The Merrifield resin used in this study were pale-yellow beads with a particle size of >50 mesh (270 μm). The Merrifield resin belongs to the macro-porous/microporous type of beads commonly used for the solid-phase synthesis of peptides and small organic molecules. They exhibited good swelling properties in CH_2Cl_2, DMF, THF, dioxane, and TFA [46]. The reactive functional group in the resin gains maximum accessibility to the reactants only when the polymer matrix swells extensively in the solvating medium. To prepare the resins, we grind Merrifield resin into particles with a particle size of 200–400 mesh (38–75 μm), then immerse 1 g of Merrifield resin in deionized water with stirring for 1 h and remove the resins from the water and dry the surface moisture. Next, the resins were soaked in DMF for 24 h to ensure full swelling and obtain a mixed solution of Merrifield resin and DMF for later use.

2.2.2. Preparation of Diamine-SQ-AER

The Diamine-SQ-AER was prepared by immobilizing diamine on Merrifield resin, as shown in Fig. 2a, and the structures of three types of Diamine-SQ-AER were presented in Fig. 2b.

Initially, the Merrifield resin/DMF mixture was allowed to settle for 1 h to eliminate excess organic solvents from the upper layer. Thereafter, three times the molar amount of diamine, specifically TEMED, DMP, or DABCO, were added to the mixture, and the resulting reaction was conducted at 60 °C with vigorous stirring for 6 h. This process led to the formation of Diamine-SQ-AER (TEMED-SQ-Cl^-, DMP-SQ-Cl^-, DABCO-SQ-Cl^-) balanced with chloride anions. During the reaction, the diamine was immobilized onto the Merrifield resin.

The excess diamine was removed from the resins through filtering and rinsing with deionized water. Subsequently, the resins were treated with 1.0 mol/L HCl and 1.0 mol/L NaOH aqueous solutions for 1 h each under constant stirring. During this process, the $-N^+(CH_3)_2H$ group reacted with OH^- to form a tertiary amine group ($-N(CH_3)_2$) along with H_2O. Furthermore, the chloride anions present in the resulting resins were exchanged by hydroxide ions. The resins were then rinsed again with a significant amount of deionized water until the solution attained neutrality. Finally, the resins were dried in an oven at 40–50 °C, and their mass was determined to calculate the yield. The current investigation yielded three distinct varieties of Diamine-SQ-AER (TEMED-SQ-OH^-, DMP-SQ-OH^-, and DABCO-SQ-OH^-) with the yields of 96 %, 93 %, and 94 %, respectively.

The synthesized resins were divided into three parts for further experiments. The first part was immersed in a 0.5 mol/L NaCl solution for 3 h under stirring conditions to facilitate ion exchange. This process was repeated six times to achieve sufficient replacement of hydroxide ions in the resin with chloride ions. The resulting resins were designated as Diamine-SQ-Cl^- resins and stored for further characterization. Similarly, the second part of the resins underwent ion exchange in a 0.5 mol/L

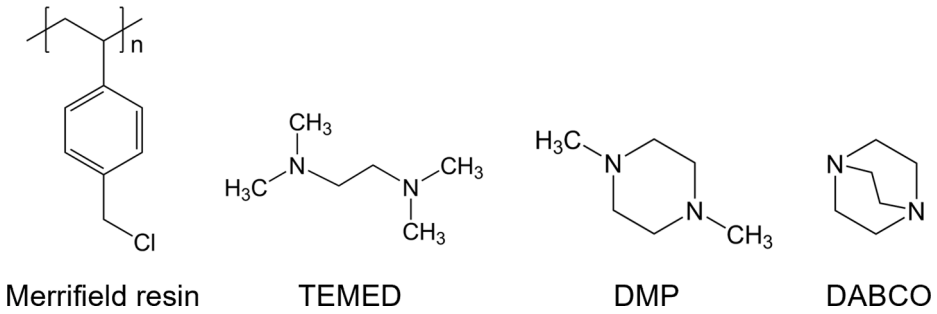

Fig. 1. Chemical structures of the Merrifield resin and diamines TEMED, DMP, and DABCO.

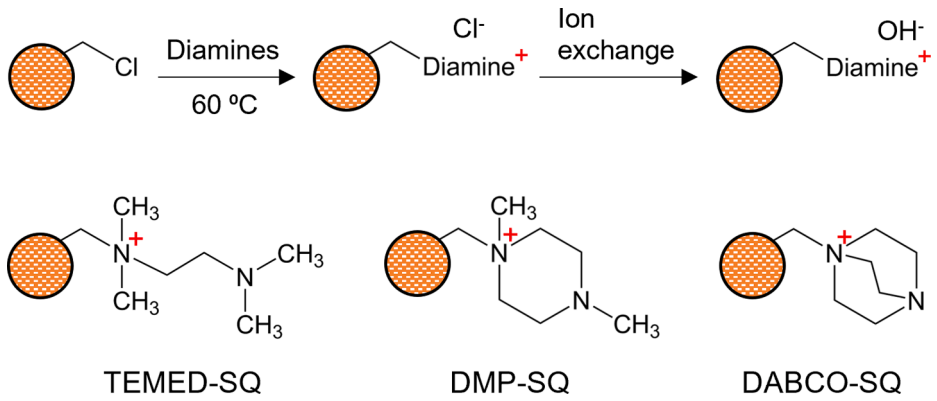

Fig. 2. (a) Preparation process of Diamine-SQ-AER (immobilization of diamine on Merrifield resin) and (b) the structure of three types of Diamine-SQ-AER.

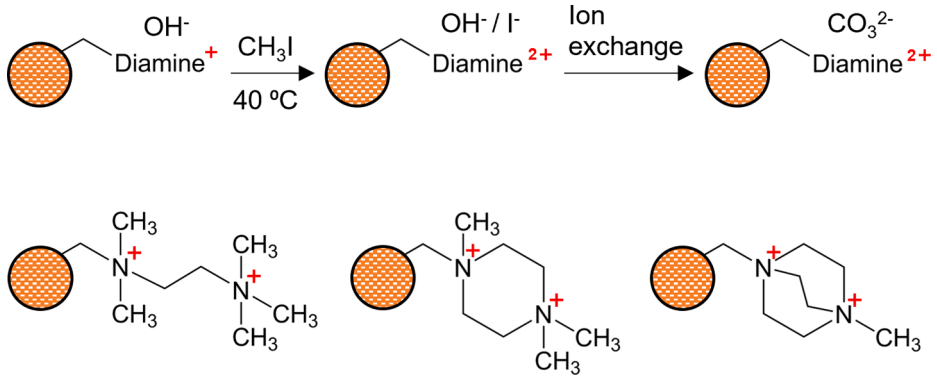

Fig. 3. (a) Preparation process of Diamine-DQ-AER (quaternization of the tertiary amine) and (b) the structure of three types of Diamine-DQ-AER.

Na_2CO_3 solution for 3 h, with the process being repeated six times to replace hydroxide ions with carbonate ions in the resin. The resultant resins were designated as Diamine-SQ-CO_3^{2-} resins and were stored for use in assessing the DAC performance. Finally, the third part of the Diamine-SQ-AER resins was used to prepare Diamine-DQ-AER.

2.2.3. Preparation of Diamine-DQ-AER

The Diamine-DQ-AER was prepared via quaternization of the tertiary amine as the 2nd step reaction after the immobilization of diamine on Merrifield resin (Fig. 2a), as shown in Fig. 3a. The structures of the prepared three types of Diamine-DQ-AER were depicted in Fig. 3b.

In this step, the tertiary amine groups on diamine were quaternized to form the second quaternary ammonium to produce Diamine-DQ-AER (TEMED-DQ-CO_3^{2-}, DMP-DQ-CO_3^{2-}, and DABCO-DQ-CO_3^{2-}) as depicted in Fig. 3a. The Diamine-SQ-OH^- resins (0.5 g) were mixed in 5 ml DMF, and then twice the molar amount of iodomethane, 0.05 g tetrabutylammonium bromide, and 5 ml of 1 mol/L NaOH aqueous solution were added into the resin/DMF mixture to react with Diamine-SQ-OH^- resins at 40 °C for 6 h. Afterward, the resins were filtered, washed with deionized water, and soaked in 1 mol/L HCl solution for 1 h and then in 1 mol/L NaOH aqueous solution for 1 h. Ion exchange was carried out by soaking and stirring part of the resins in 0.5 mol/L NaCl solution to obtain Diamine-DQ-Cl^- resins, while the rest were soaked and stirred in Na_2CO_3 solution to obtain Diamine-DQ-CO_3^{2-} resins. The resulting Diamine-DQ-Cl^- and Diamine-DQ-CO_3^{2-} resins were dried in an oven at 40–50 °C and stored for further characterization and testing.

2.3. Characterization of anion-exchange resins

The morphologies of the resins were analyzed using SEM (Zeiss-Supra 55VP-FEG-SEM). The samples were dried and ground, then mounted in a sample holder and coated with a thin gold layer to make the samples electronically conductive. The measurement of element content was performed on EDS (EDAX OCTANE PRO-A EDS detector) to

analyze the elemental chlorine of Merrifield resins and Diamine-SQ/DQ-Cl^- resins. Thermal stability tests for the Merrifield resins and the Diamine-DQ-CO_3^{2-} resins were performed by TGA (TG 209F1 Libre, Netzsch). Samples with a weight of 5–10 mg were placed in a porcelain crucible and heated from room temperature to 800 °C with a heating rate of 5 °C/min. Nitrogen was used as both protective and sweep gas. The FT-IR spectroscopy was performed for all chemicals and resultant resins by using a Thermo Nicolet Nexus spectrometer with a smart endurance reflection cell. The obtained spectra of all samples were in the mid-IR region with wavenumber ranging from 550 cm^{-1} to 4000 cm^{-1}.

2.4. CO_2 adsorption/desorption test

Fig. 4 depicts the experimental setup used to measure the CO_2 adsorption–desorption performance of the Diamine-SQ/DQ-AER. The system consists of a closed, temperature and humidity-controlled sample chamber with a volume of 2.68 L. A CO_2 detector (MI70 Measurement Indicator, Vaisala, 0–5000 ppm) is used to monitor CO_2 concentration in real-time and record data automatically. The chamber is connected to a dry air tank (controlled by valve 1), and deionized water can be pumped into the bottom of the sample chamber (controlled by valve 2). Gas outlet valve 3 is used when dry air or deionized water flows into the chamber. A rotor, located at the bottom of the chamber, is used in conjunction with a heating stirring platform to accelerate the humidification process, ensure uniform gas diffusion, and maintain the desired temperature.

CO_2 adsorption was enabled by introducing the dry air flow controlled by valves 1 and 3. The adsorption environment contained 400 ppm CO_2 with a temperature of 25 °C and relative humidity of <0.5 % under atmospheric pressure. The adsorption process lasts over 12 h to ensure sufficient loading/adsorption of CO_2 to the sample. Desorption was triggered by evaporation humidification (25 °C) when deionized water (already at equilibrium with 400 ppm CO_2) was pumped into the bottom of the sample chamber (controlled by valve 2). Then the detector records the concentration data in the chamber every 30 s with a resolution of 10 ppm, and the obtained data is processed into desorption kinetics curves by the moving average method.

It is worth noting that leak detection of the system was conducted before the experiment to ensure the reliability and accuracy of the experimental results. The results (see Figure S1) indicate that the CO_2 leakage rate of the experimental system was negligible for all initial CO_2 concentrations tested. More details can be found in the Supplementary Information (SI). In order to maintain a constant experimental condition for all CO_2 adsorption–desorption performance tests, the initial CO_2 concentration in the system was kept at 400 ppm, similar to atmospheric CO_2 concentration, and the initial relative humidity in the system was adjusted to <0.5 % at 25 °C through flow control of the dry air tank. After stabilizing for 1 h, 530 ml of deionized water was pumped into the chamber with all valves to the sample chamber closed and the rotor inside activated to increase the humidity and initiate the CO_2 release

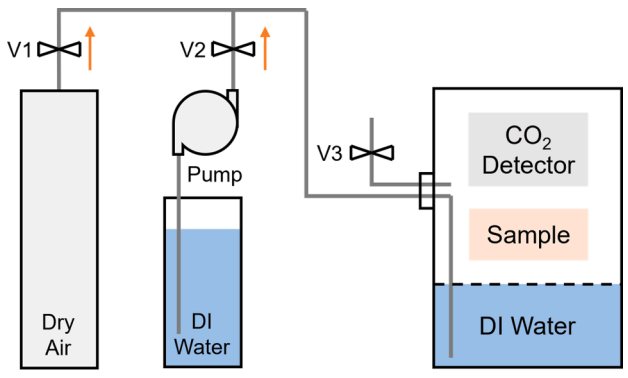

Fig. 4. CO_2 adsorption-desorption experimental system.

process. The ad-/desorption capacity of the sample, denoted as "*C*," was calculated using the following equation:

$$C = \frac{(V_t - V_w) \times \Delta c}{24.5\ m} \times 10^{-3} \quad mmol/g \tag{2}$$

where V_t is the total volume of the system, V_w is the volume of water used during the test, Δc is the difference in CO_2 concentration before and after the test, and m is the mass of the sample. All resin samples tested had a particle size of 200–400 mesh (38–75 μm).

3. Results and discussions

3.1. Optimization of testing conditions

Two control experiments were conducted to optimize the testing conditions and procedure for all CO_2 adsorption/desorption experiments in this work. The first experiment examined the CO_2 desorption performance of different masses of commercial resin IRA-900 at a CO_2 concentration of 500 ppm. Desorption equilibrium was considered achieved when the CO_2 concentration remained stable for 10 min.

Results in Fig. 5a show that the CO_2 concentration to reach the desorption equilibrium in the chamber increases with the mass of the resin, while the CO_2 desorption capacity decreases accordingly (Fig. 5b and solid purple line in Fig. 5c). Interestingly, the increase of sample mass did not result in a linear increase in CO_2 concentration difference (ΔCO_2), as seen in Fig. 5c. The red dotted line in the figure indicates the theoretical value of ΔCO_2 under ideal desorption conditions, while the black line shows the test result of ΔCO_2. A higher agreement between the red dotted line and the black solid line was observed when the ΔCO_2 was lower than 250 ppm (indicated by red dots). The actual concentration of CO_2 in the chamber is 750 ppm when the ΔCO_2 is 250 ppm. When the ΔCO_2 exceeded 250 ppm, the deviation between the test result and the theoretical value gradually increased (indicated by black dots), indicating that the released CO_2 increased the partial pressure of CO_2 in the chamber, which somewhat hindered the further desorption of the resin. The inhibitory effect became more prominent when the ΔCO_2 varied over 250 ppm. Thus, it is important to use the appropriate weight of materials (or effective functional group content) in CO_2 test systems to avoid excessively high CO_2 partial pressure that would inhibit the material from fully desorbing CO_2 so as to achieve the optimal performance and measure the real CO_2 ad-/desorption capacity of materials.

The desorption capacities of IRA-900 resin weighing 0.025 g were also investigated at varying initial CO_2 concentrations. The resin demonstrates the ability to desorb CO_2 at various CO_2 concentrations, as shown in Fig. 5d, albeit with a decreasing desorption capacity as the initial CO_2 concentration increasing (Fig. 5e). Notably, the results presented in Fig. 5f reveal a sharp reduction in the CO_2 desorption capacity of the resin when the initial CO_2 concentration exceeds 1000 ppm. At a CO_2 concentration of 2000 ppm, over 70 % of the CO_2 desorption capacity was lost. Both the released CO_2 during the test and the CO_2 in the chamber at the outset of the experiment may create a high partial pressure of CO_2 that inhibits the desorption process of the resin. To counteract this effect, a preliminary prediction of material properties based on effective functional group content should be made during testing. We suggest maintaining the CO_2 concentration in the chamber at or below 750 ppm and selecting the appropriate weight of test material to reduce the inhibitory effect of CO_2 partial pressure on the desorption process of the material, ultimately measuring the true CO_2 desorption capacity of the material. The optimized test parameters are summarized in Table 1.

3.2. Structural and chemical characteristics of the resins

The surface and cross-section SEM images of TEMED-DQ-AER are presented in Fig. 6. The original morphology of the resin exhibits a smooth and spherical surface, as shown in Fig. 6a. Part of the resin was

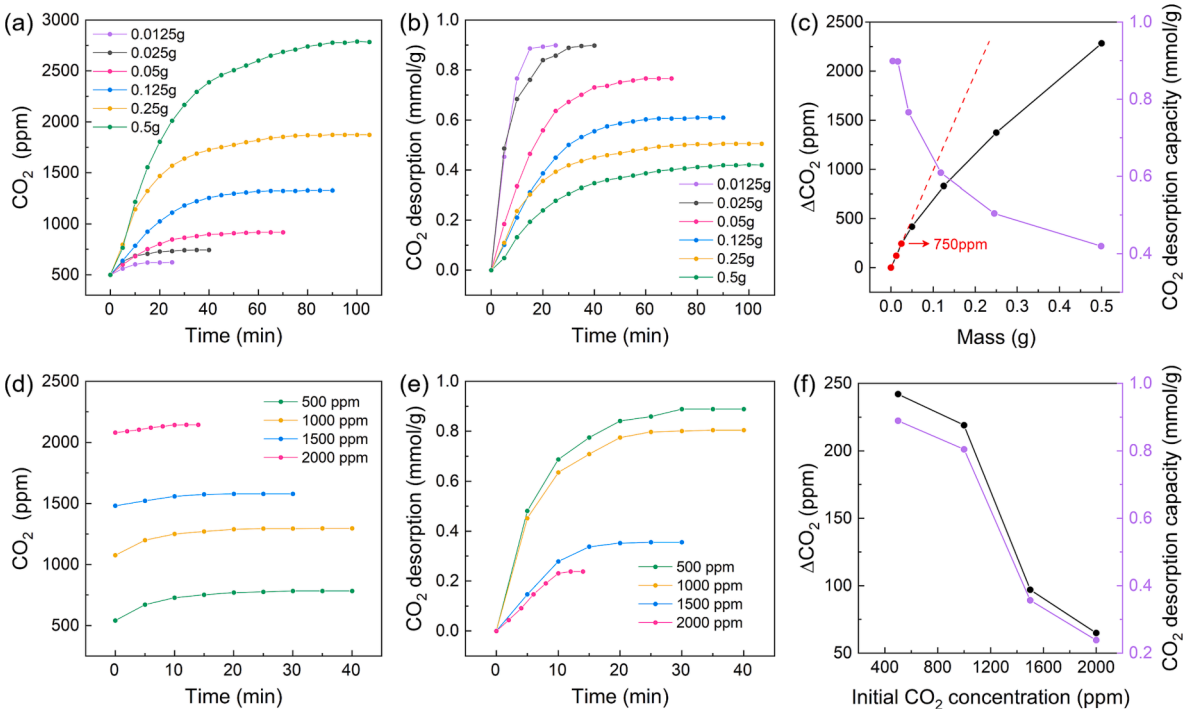

Fig. 5. (a) Change of CO_2 concentration in test system with different material masses, (b) CO_2 desorption kinetic curves of different material masses, (c) CO_2 concentration difference and CO_2 desorption capacity change with material mass, (d) CO_2 concentration change curve under different initial CO_2 concentrations, (e) CO_2 desorption kinetics curves under different initial CO_2 concentrations, and (f) CO_2 concentration difference and CO_2 desorption capacity change with initial CO_2 concentration.

Table 1
Summary of the optimized testing parameters.

Temperature	Pressure	Relative humidity	CO_2 concentration
25 °C	Atmospheric condition	<0.5 % (initial) >99 % (test)	~400 ppm (initial) <750 ppm (test)

ground to expose its internal structure, revealing a similar morphology and internal structure for other Diamine-SQ/DQ-AER and Merrifield resin, suggesting that the loading of functional groups and quaternarization have little effect on the resin structure. The resin used in this study was the macro-porous resin [35], as observed from the cross-section at the scale of 1 μm in Fig. 6c, showing an evident pore structure.

The chlorine content of Diamine-SQ/DQ-Cl^- resins was estimated by conducting elemental analysis to evaluate the functional group loading and estimating the theoretical limit of CO_2 adsorption capacity, which is approximately 16.73 %. The carbon, nitrogen, and chlorine content of Merrifield resin and Diamine-SQ/DQ-Cl^- resins were presented in Table 2. Notably, the nitrogen content in Diamine-SQ-Cl^- resins

Table 2
Elemental contents of the Merrifield resin and Diamine-SQ/DQ-Cl^- resins.

Resin	C (wt%)	N (wt%)	Cl (wt%)	Cl (mmol/g)
Merrifield resin	83.27	0.00	16.73	4.71
TEMED-SQ-Cl^-	79.62	5.80	14.57	4.11
TEMED-DQ-Cl^-	69.99	5.37	24.64	6.94
DMP-SQ-Cl^-	79.76	6.92	13.32	3.75
DMP-DQ-Cl^-	70.25	5.74	24.01	6.76
DABCO-SQ-Cl^-	77.74	8.06	14.20	4.00
DABCO-DQ-Cl^-	66.72	7.54	25.73	7.25

increased significantly from 0 to 5.80–8.06 % after diamine immobilization, indicating the successful anchoring of diamine in the resin. Furthermore, the chlorine content of Diamine-DQ-Cl^- resins (6.76–7.25 mmol/g) was found to be substantially higher than that of the corresponding Diamine-SQ-Cl^- resins (3.75–4.11 mmol/g). This increase in chlorine content (68–81 %) suggests that the yield of Diamine-DQ-Cl^- resins reached 68–81 % during the quaternization process. Based on

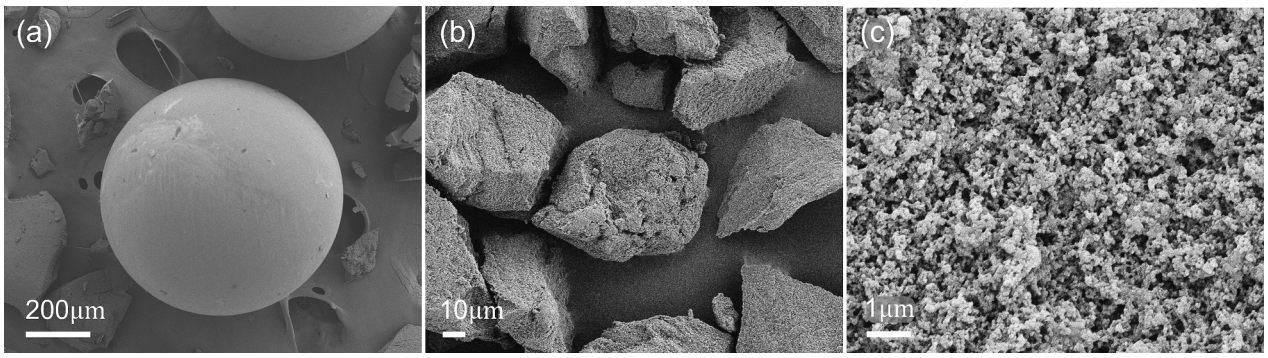

Fig. 6. SEM images of the TEMED-DQ-AER at different scales: (a) the original resin, (b) the resin after grounding, and (c) an enlarged view of the cross-section.

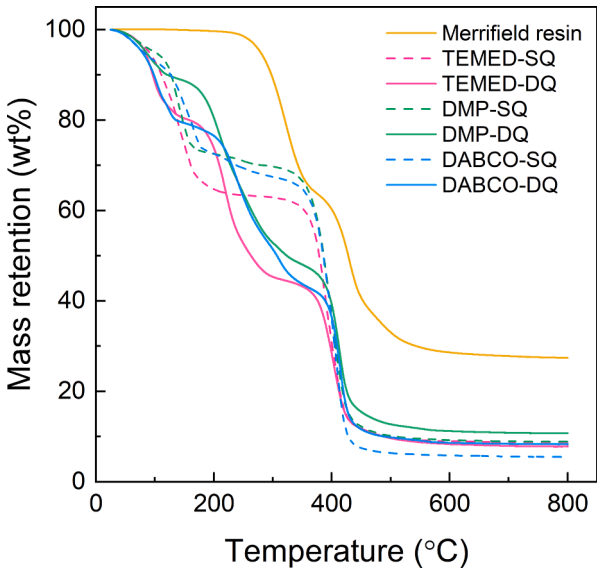

Fig. 7. Thermal stabilities of Merrifield resin and Diamine-SQ/DQ-CO_3^{2-} resins.

these findings, the ion exchange capacity of Diamine-DQ-AER is approximately 1.68–1.81 times that of Diamine-SQ-AER, which also implies that Diamine-DQ-AER has higher functional group content and CO_2 adsorption capacity.

The thermal behavior of the Merrifield resin and Diamine-SQ/DQ-CO_3^{2-} resins were analyzed using TGA, as shown in Fig. 7. The results show that the weight loss observed before the temperature reached 100 °C in all Diamine-SQ/DQ-CO_3^{2-} resins due to the presence of hydrophilic tertiary amine and quaternary ammonium groups in the resin, which absorb water molecules, whereas Merrifield resin does not show significant weight loss until ~270 °C, indicating the absence of hydrophilic groups in Merrifield resin. Previous studies have demonstrated that weight loss at around 200 °C in anion-exchange resins is due to the loss of decomposition products associated with the quaternary ammonium functional groups of the resin, and carbonaceous species are liberated at around 350 °C [47,48]. Therefore, the weight loss of the Diamine-SQ/DQ-CO_3^{2-} resins in the range of 70–350 °C is due to the degradation of functional groups. Specifically, the quaternary ammonium-tertiary amine groups of Diamine-SQ-CO_3^{2-} resin starts to degrade at around 95 °C, with a significant amount of degradation occurring between 110 and 200 °C. The degradation rate gradually decreases until ~270 °C. While Diamine-DQ-CO_3^{2-} resins show two large-scale weight loss processes due to the degraded functional groups, including the same quaternary ammonium groups as Diamine-SQ-CO_3^{2-} resins and new quaternary ammonium groups generated by quaternization of tertiary amines. Notably, the first degradation process of Diamine-DQ-CO_3^{2-} resin began at 70–80 °C with the highest degradation rate around 100 °C, indicating poor thermal stability of the second formed quaternary ammonium groups. The degradation temperature of Diamine-SQ/DQ-CO_3^{2-} resin is relatively low compared with Merrifield resin, which further indicates that a high degree of quaternization can lead to a decrease in the thermal stability of the resin. Based on the tested TGA results, we suggest that the working temperature of Diamine-SQ/DQ-CO_3^{2-} resin should be below 70 °C, which is not a problem for applications in DAC as it usually operates at room temperature.

The weight loss of each stage is summarized in Table S1 to provide more detailed information on the thermal behavior of Merrifield resin and Diamine-SQ/DQ-CO_3^{2-} resins. The data show that the initial chlorine content of Merrifield resin was 4.71 mmol/g, with the mass of chloromethyl (–CH_2-Cl) equivalent to 23.3 % of the resin mass, which corresponds to 30.8 % weight loss of Merrifield resin in the temperature

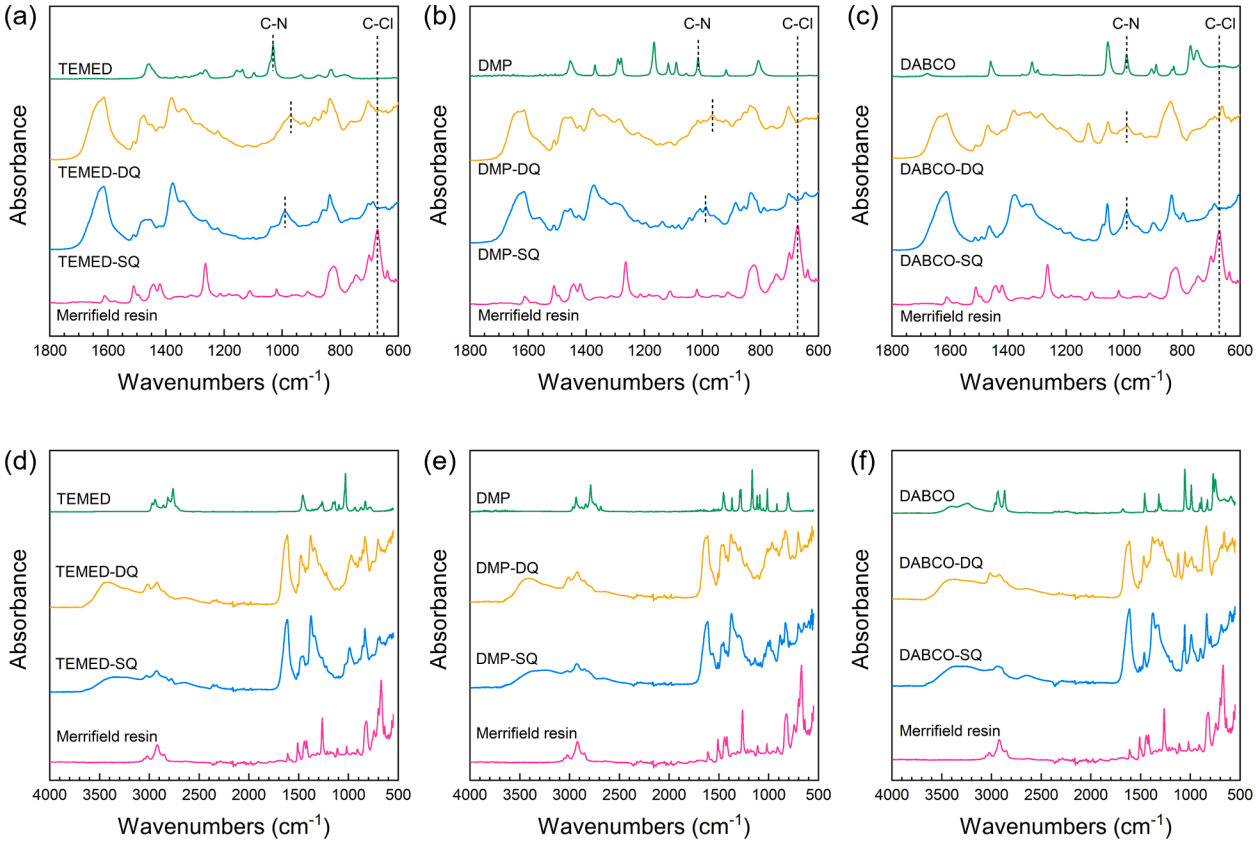

Fig. 8. FT-IR spectra comparison among the diamine, Diamine-SQ/DQ-CO_3^{2-}, and Merrifield resin. (a), (b) and (c) are the enlarged view of (d), (e), and (f), respectively, with the wavenumber in the range of 600–1800 cm^{-1}.

range of 270–365 °C attributed to in the degradation of chloromethyl. Moreover, Diamine-DQ-CO_3^{2-} resins exhibited a higher percentage of functional group weight loss than Diamine-SQ-CO_3^{2-} resins, indicating successful implementation of the quaternization reaction and increased loading of functional groups.

FT-IR spectral analysis of Merrifield resin and Diamine-SQ/DQ-CO_3^{2-} were performed to further elucidate the structure of the diamines, and the results are shown in Fig. 8. The FT-IR spectrum of Merrifield resin shows peaks in the region of 650–700 cm^{-1}, which can be attributed to C—Cl stretching, while the peak at 1265 cm^{-1} corresponds to C—H wagging in the CH_2—Cl group [48]. Additionally, the appearance of the peak at around 1615 cm^{-1} is due to aromatic C═C stretching [49]. The C—Cl stretching and CH_2—Cl wagging peaks observed in Merrifield resin disappear completely for the Diamine-SQ/DQ-CO_3^{2-} resins, and, instead, a new peak emerges at around 1000 cm^{-1}, corresponding to the asymmetric stretching of C—N in the Diamine-SQ/DQ-CO_3^{2-} resins [50]. This confirms the complete quaternization of the CH_2—Cl group during the process of the immobilization of diamine on Merrifield resin. Additionally, the peak at around 1370 cm^{-1} in the spectrum of Diamine-SQ/DQ-CO_3^{2-} resins is due to the asymmetrical in-plane stretch of the carbonate ion [51]. Furthermore, the broad peak at 3100–3500 cm^{-1} can be attributed to the O—H vibration of water, which is favored by the hydrophilic quaternary ammonium groups in Diamine-SQ/DQ-CO_3^{2-} resins. Conversely, Merrifield resin does not contain carbonate ions or hydrophilic groups, and no peak was detected in this range.

3.3. Optimization of resin material synthesis conditions

The effects of synthesis conditions were studied to optimize the synthesis process of resin materials. The chlorine content of the Merrifield resin used in this experiment was approximately 11.33 %, and the reaction time, reaction temperature, and drying temperature were set as 6 h, 30–80 °C, and 40 °C, respectively. The effects of temperatures on the efficiency of immobilization of diamine on Merrifield resin in the first step (to make Diamine-SQ-Cl^- resins) and of quaternization of the tertiary amine in the second step (to make Diamine-DQ-Cl^- resins) are shown in Fig. 9 by analyzing the chlorine content of resins in each pair of the experiments.

As shown by the dotted line in Fig. 8a, the chlorine content of the TEMED-based Diamine-SQ-Cl^- resins shows a slight increase as the first reaction temperature rises from 30 °C to 60 °C. Upon further temperature increase to 80 °C, the chlorine content remains relatively stable, indicating that the yield of the first reaction stabilizes from 60 °C onwards. This increase in chlorine content before 60 °C may be attributed to the favorable effects of temperature on resin swelling, diffusion and flow of reactant molecules, compatibility of reactants with organic solvents, and collisions with the resin. With regard to the second reaction (solid line in Fig. 8a), the chlorine content of the TEMED-based Diamine-DQ-Cl^- resins increases and reaches its maximum when the temperature rises from 30 °C to 40 °C, indicating the maximum quaternization efficiency. However, as the temperature continues to increase, the chlorine content decreases significantly and then stabilizes at 70 °C and onwards because that at temperatures exceeding 40 °C, the temperature reaches the boiling point of the iodomethane solution (41–43 °C), leading to the evaporation of reactants in the system, which reduces the reaction rate, causing incomplete reactions and a significant decrease in the efficiency of quaternization, and resulting in lower yields. The DMP and DABCO-based Diamine-DQ-Cl^- resins exhibit a similar trend, suggesting that the reaction temperature has a significant effect on the synthesis of the desired materials. Overall, the optimal results in terms of chlorine content, quaternization efficiency, and yield were obtained when the first reaction was carried out at 60 °C and the second reaction at 40 °C.

3.4. Direct air capture performance

Cyclic CO_2 adsorption–desorption tests were conducted in the sample chamber presented in Fig. 4. A group of the recorded CO_2 desorption kinetic curves within 4.5 days of the 6 types of as-prepared resins is shown in Fig. 10a. The solid and dashed lines represent the desorption kinetic curves of Diamine-DQ-CO_3^{2-} and Diamine-SQ-CO_3^{2-}, respectively. The pink, green, and blue colors indicate that the resin is formed by the treatment of three chemicals, namely TEMED, DMP, and DABCO, which are referred to as TEMED-based, DMP-based, and DABCO-based resins, respectively. Fig. 10b, 11, and 12 also adopt the same representation method.

The CO_2 desorption process exhibited a similar pattern for all samples, which can be divided into two distinct stages. To obtain the time-CO_2 desorption rate curve, we took the first derivative of the CO_2 desorption kinetic curve with respect to time, as shown in Fig. 10b, where the desorption rate change within 0–500 min is presented. At around 120 min, the desorption rate of all samples decreased sharply to a small value (<0.0025 mmol/(g·min)). Therefore, we defined the desorption process before 120 min as the first stage of CO_2 desorption, and the part after 120 min as the second stage of CO_2 desorption. The complete desorption rate change for 4.5 days is shown in Figure S2. The orange-shaded part in Fig. 10a represents the first stage of CO_2 desorption, during which CO_2 was rapidly released from the material when moisture quickly diffuses to the surface of the sample. In the second stage, the CO_2 desorption rate decreased significantly, probably because it is much more difficult for moisture to diffuse into the resin's core and its interior small pores. The slow desorption process was allowed for a long time of up to 114 h (6840 min) to measure the resin's final desorption capacity.

The CO_2 adsorption capacities of the as-prepared sorbents and a CO_2 sorbent with the highest moisture-swing adsorption capacity reported in the literature (QCPS-2/PES) [40] are presented in Fig. 11. In this work, each sample was tested for at least 3 adsorption–desorption cycles to obtain the average adsorption capacity. The capacity of the as-prepared TEMED-DQ-AER, DMP-DQ-AER, and DABCO-DQ-AER reached 3.41,

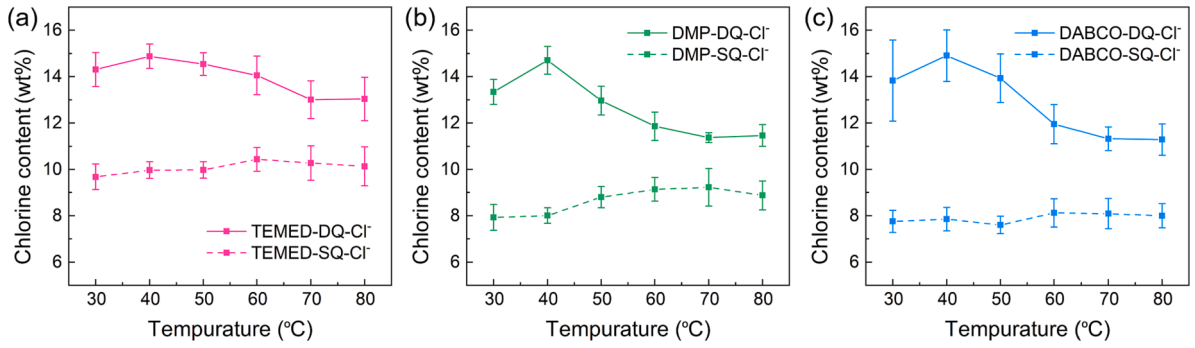

Fig. 9. Chlorine content of Diamine-SQ/DQ-Cl^- resins synthesized at different temperatures. (a), (b), and (c) represent the test results of TEMED-based, DMP-based, and DABCO-based AER, respectively.

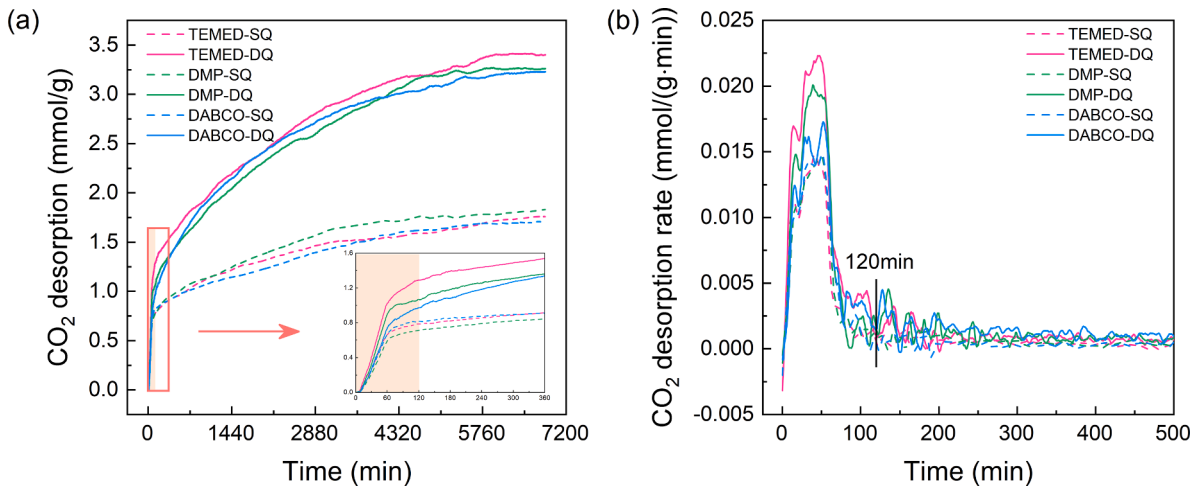

Fig. 10. (a) CO_2 desorption kinetics curves of Diamine-SQ/DQ-CO_3^{2-} resins, (b) the desorption rate change within 0–500 min of Diamine-SQ/DQ-CO_3^{2-} resins.

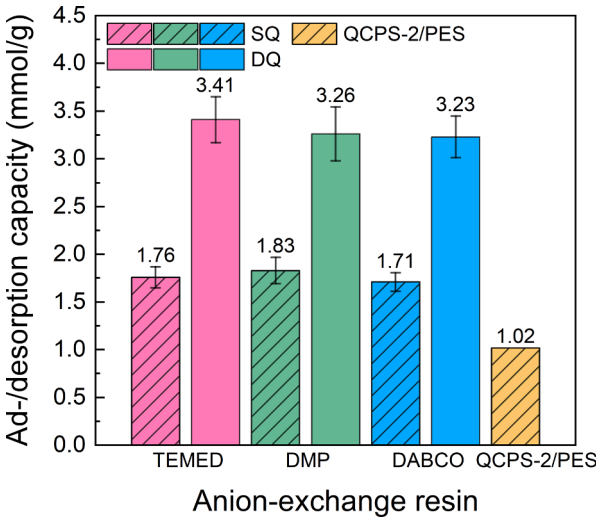

Fig. 11. The CO_2 sorption capacity of Diamine-SQ/DQ-CO_3^{2-} resins and a CO_2 sorbent reported in the literature.

3.26, and 3.23 mmol/g at 25 °C and atmospheric pressure, which were, respectively, 1.94, 1.78, and 1.88 times that of the corresponding Diamine-SQ-AER (1.76, 1.83, and 1.71 mmol/g), owing to the increased quaternary ammonium content in Diamine-DQ-CO_3^{2-} resins. The theoretical limit of CO_2 adsorption capacity and the responding chlorine content and carbonate content, and the measured capacity of various types of resins are listed in Table 3. As expected, the measured sorption capacity of the resin is close to the theoretical limit, which is due to the optimized testing conditions with good sealing and our improved method that avoids the influence of CO_2 partial pressure on the test results.

Fig. 12a compares the CO_2 sorption capacity of the MSDACS in this work with those reported in the literature, including commercial single quaternary ammonium resins (indicated by purple dots) and other MSDACS (indicated by black dots). The desorption half-time (the time to reach half of the capacity) has been used as an empirical index of the desorption kinetics [52]. As the adsorption and desorption half-time are usually close [35,41], we consider that it is reasonable to present and compare the adsorption and desorption half-time together, as also shown in Fig. 12. The Diamine-DQ-CO_3^{2-} resin developed in this work exhibits the highest CO_2 sorption capacity (~3.41 mmol/g of TEMED-DQ-AER). However, the Diamine-DQ-CO_3^{2-} resin also shows the slowest kinetics as its desorption half-time is the longest (607 min of TEMED-DQ-AER). It is worth noting that adsorption/desorption kinetics can be influenced by the scale and flow rate of the testing system. For example, in Armstrong et al.'s work [53], where a closed circulation system with a volume of 0.175 L and an airflow rate of 1 L/min (enable by a circulation pump) was used, in merely 1 min, the gas inside the testing system was circulated over 5 times, which strongly promoted the diffusion, humidification, and adsorption/desorption processes. Since we used a static desorption system (almost zero air flow rate) with a volume of 2.68 L and the humidification process was realized only by water evaporation from the deionized water surface in the sample chamber at room temperature, it is understandable that it took longer time for desorption to reach equilibrium. As at this moment, we are focused more on improving the CO_2 sorption capacity of DAC sorbents, no other measures were taken to increase the desorption rate.

Upon analyzing the data of each material presented in Fig. 12b, it was observed that the CO_2 sorption capacity of commercial resins and other MSDACS could reach up to 1.02 mmol/g, with a half-time that usually does not exceed 80 min. This indicates a significant advantage in ad-/desorption kinetics compared to the half-time presented of TEMED-DQ-CO_3^{2-} resin in this work. However, this advantage can be attributed to different definitions of ad-/desorption equilibrium time researchers use. For instance, Wang et al. [35] defined the desorption equilibrium as

Table 3
The anion content and the DAC performance of the resins used in the present work.

Sample	Cl^- content after ion exchange (mmol/g)	CO_3^{2-} content after ion exchange (mmol/g)	The theoretical limit of CO_2 ad-/desorption capacity (mmol/g)	CO_2 desorption capacity as measured (mmol/g)
TEMED-SQ	4.11	2.055	2.055	1.76
TEMED-DQ	6.94	3.470	3.470	3.41
DMP-SQ	3.75	1.875	1.875	1.83
DMP-DQ	6.76	3.380	3.380	3.26
DABCO-SQ	4.00	2.000	2.000	1.71
DABCO-DQ	7.25	3.625	3.625	3.23

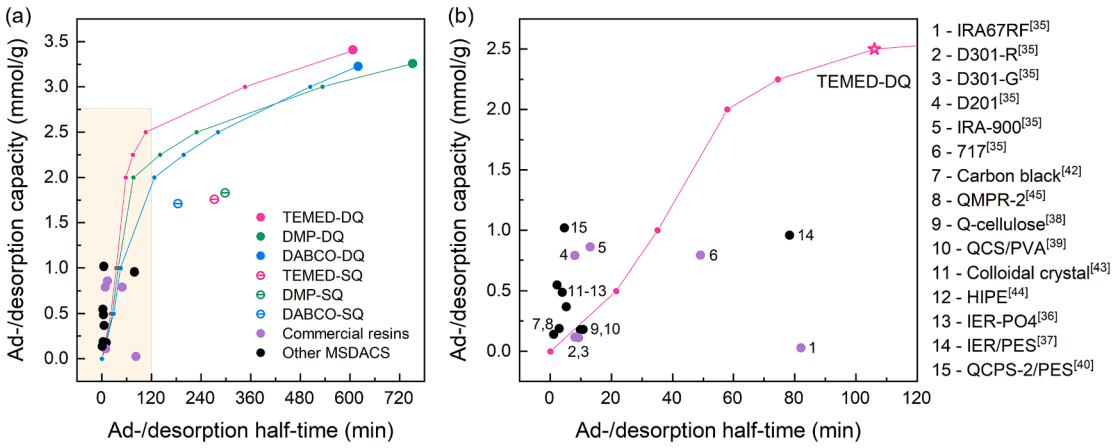

Fig. 12. (a) The ad-/desorption half-time and capacity of the Diamine-SQ/DQ-CO_3^{2-} resins developed in this work and other MSDACS reported in the literature. (b) Enlarged view of the yellow-shaded part in Fig. 12a within the half-time range of 120 min. (For interpretation of the references to colour in this figure legend, the reader is referred to the web version of this article.)

the point where CO_2 concentration in the system does not change significantly within 20 min, which greatly shortens the test time and yields a smaller half-time and better kinetic results. Nevertheless, the CO_2 desorption kinetic curve in Fig. 10a indicates that a large amount of ad-/desorption capacity remained undetected due to the test time of the previous studies being mainly concentrated in the first stage of the process. Therefore, the ad-/desorption capacity measured in the experiment was lower than the theoretical ad-/desorption capacity. For instance, the test adsorption capacity of commercial resin IRA-900 was only 45 % of the theoretical adsorption capacity of 1.85 mmol/g [35]. The second stage of the process has not yet been investigated in terms of performance testing. The desorption kinetics data presented in the orange-shaded part in Fig. 10a demonstrate the rapid CO_2 desorption process of the Diamine-SQ/DQ-CO_3^{2-} resins in the first stage. Specifically, after 120 min, the desorption capacity for the three Diamine-DQ-CO_3^{2-} resins were 1.29 mmol/g, 1.07 mmol/g, and 0.97 mmol/g, corresponding to approximately 38 %, 33 %, and 30 % of the total desorption capacity. These findings suggest that the amount of CO_2 desorbed by the three resins in the second stage reached approximately 62 %, 67 %, and 70 % of the total adsorption capacity, respectively. Thus, the performance test conducted in the second stage plays a crucial role in determining the actual total ad-/desorption capacity of the material.

In assessing the desorption efficiency of a material, reliance on half-time measurements can be problematic as it fails to account for differences in total test time. To address this, we marked the half-time of the resin when the ad-/desorption capacity reached specific values and connected them with correspondingly colored lines in Fig. 12. The relationship between ad-/desorption half-time and capacity displays two distinct stages, with a sharp increase in half-time occurring after the ad-/desorption capacity reaches 2.50 mmol/g. Fig. 12b, which shows the data distribution diagram of the material within the half-time range of 120 min, illustrates that the desorption efficiency of TEMED-DQ-AER improves markedly when the desorption capacity is between 0 and 2.50 mmol/g, with a maximum half-time of 106 min. At a desorption capacity of 2.00 mmol/g, the half-time is only 58 min, which is comparable to that of other materials although the sorption capacity is much higher. Despite not reaching desorption equilibrium, the desorption capacity of TEMED-DQ-AER at this point still presents a substantial advantage over other materials, being more than twice that of other materials. To achieve optimal material utilization, it is necessary to further evaluate the use efficiency of materials at various stages in real-work scenarios. Detailed data on the ad-/desorption capacity and half-time of all materials can be found in Table S2.

The cyclic DAC performance of TEMED-DQ-CO_3^{2-} resins was

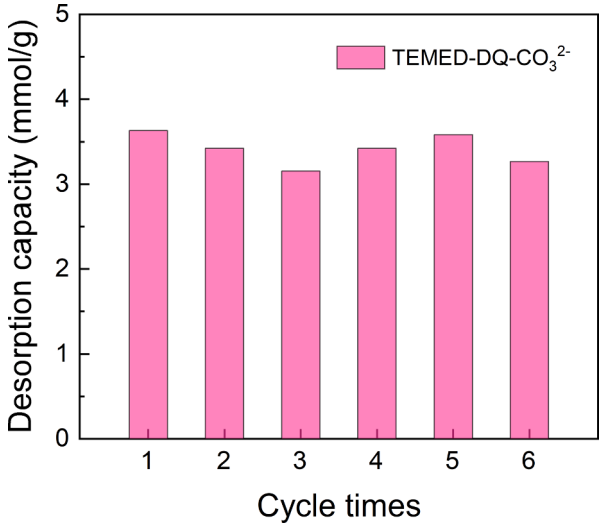

Fig. 13. Six CO_2 desorption-adsorption cycles of the TEMED-DQ-CO_3^{2-}.

evaluated through six consecutive CO_2 desorption-adsorption tests at room temperature and pressure, as shown in Fig. 13. The cycle number of six was determined based on the literature [26,36,40], which is a common practice in the field of DAC sorbent research and development. For example, Sun et al. conducted cycle tests on commercial single quaternary ammonium resins for 20 cycles without significant performance degradation [54]. Considering that the double quaternary ammonium resin developed in our work represents an improvement upon anion exchange resin and exhibits similar chemical structure stability to commercial single quaternary ammonium resin, it is reasonable to expect it to exhibit similar cyclic performance. Furthermore, moisture-swing adsorbents operate under normal temperature and pressure conditions, where the microstructure and chemical structure are minimally affected by temperature and pressure variations. Hence, a larger cycle number is not necessary or expected to provide additional information in this study.

The results indicate that the desorption capacity of the resin remained stable between 3.15 and 3.63 mmol/g throughout the six cycles of desorption-absorption process by moisture-swing. No significant performance degradation was observed. These findings highlight the potential of TEMED-DQ-CO_3^{2-} resins as a promising candidate for practical applications in carbon capture and storage, providing an effective and sustainable solution to mitigate CO_2 emissions.

4. Conclusion

In this study, the double quaternary ammonium strategy was applied and proven as an effective solution for enhancing the CO_2 sorption capacity of DAC sorbents. Diamine-DQ-AER was developed by modifying Merrifield resin with tertiary diamines such as TEMED, DMP, and DABCO, exhibiting significantly enhanced DAC capacity, i.e., a CO_2 capacity of ~3.41 mmol/g at room temperature and atmospheric conditions, ~1.94 times higher than that of Diamine-SQ-AER. Moreover, Diamine-DQ-AER shows a stable DAC capacity in the 6-cycle test, tripled that of MSDACS reported in the literature (up to 1.02 mmol/g). We have also optimized the testing conditions and procedure, and measured the real CO_2 desorption capacity of the sorbents and the complete desorption kinetic curve more precisely, revealing a two-stage desorption process, where the material displayed good desorption kinetics in the first stage. The performance proves that incorporating multiple active sites has the potential to develop high-capacity moisture-swing sorbents, providing a promising solution for enhancing DAC performance. In the future, we will further optimize the operating parameters and study the CO_2 adsorption/desorption kinetics to improve the efficiency of the material and promote the practical application of MSDACS in the field of DAC.

CRediT authorship contribution statement

Xueru Wang: Conceptualization, Methodology, Formal analysis, Validation, Investigation, Writing – review & editing, Visualization. **Yan Chen:** Writing – review & editing. **Wenqi Xu:** Writing – review & editing. **Arne Lindbråthen:** Writing – review & editing. **Xinyue Cheng:** Writing – review & editing. **Xi Chen:** Supervision, Writing – review & editing. **Liangliang Zhu:** Funding acquisition, Supervision, Writing – review & editing. **Liyuan Deng:** Funding acquisition, Supervision, Writing – review & editing.

Declaration of Competing Interest

The authors declare that they have no known competing financial interests or personal relationships that could have appeared to influence the work reported in this paper.

Data availability

Data will be made available on request.

Acknowledgments

This work was supported by the National Natural Science Foundation of China (12002271), the Young Talent Support Program of Xi'an Science and Technology Association (095920221368), the Research Council of Norway (No. 294533), and China Scholarship Council (CSC).

Appendix A. Supplementary material

Supplementary data to this article can be found online at https://doi.org/10.1016/j.seppur.2023.124489.

References

[1] H.R. Stuart, Carbon capture and storage: how green can black be? Science 325 (5948) (2009) 1647–1652.
[2] IPCC, 2021: Summary for Policymakers. In: Climate Change 2021: The Physical Science Basis. Contribution of Working Group I to the Sixth Assessment Report of the Intergovernmental Panel on Climate Change [Masson-Delmotte, V., P. Zhai, A. Pirani, S.L. Connors, C. Péan, S. Berger, N. Caud, Y. Chen, L. Goldfarb, M.I. Gomis, M. Huang, K. Leitzell, E. Lonnoy, J.B.R. Matthews, T.K. Maycock, T. Waterfield, O. Yelekçi, R. Yu, and B. Zhou (eds.)].
[3] P. Markewitz, W. Kuckshinrichs, W. Leitner, J. Linssen, P. Zapp, R. Bongartz, A. Schreiber, T.E. Müller, Worldwide innovations in the development of carbon capture technologies and the utilization of CO 2, Energ. Environ. Sci. 5 (6) (2012) 7281–7305.
[4] K.M.K. Yu, I. Curcic, J. Gabriel, S.C.E. Tsang, Recent advances in CO2 capture and utilization, ChemSusChem: Chem. Sustain. Energy Mater. 1(11) (2008) 893-899.
[5] C.-H. Yu, C.-H. Huang, C.-S. Tan, A review of CO2 capture by absorption and adsorption, Aerosol Air Qual. Res. 12 (5) (2012) 745–769.
[6] W.Y. Hong, A techno-economic review on carbon capture, utilisation and storage systems for achieving a net-zero CO2 emissions future, Carbon Capture Sci. Technol. (2022), 100044.
[7] K.S. Lackner, S. Brennan, J.M. Matter, A.-H.A. Park, A. Wright, B. Van Der Zwaan, The urgency of the development of CO2 capture from ambient air, Proc. Nat. Acad. Sci. 109(33) (2012) 13156-13162.
[8] M. Mostafa, C. Antonicelli, C. Varela, D. Barletta, E. Zondervan, Capturing CO2 from the atmosphere: Design and analysis of a large-scale DAC facility, Carbon Capt. Sci. Technol. 4 (2022), 100060.
[9] X. Shi, Y. Lin, X. Chen, Development of sorbent materials for direct air capture of CO2, MRS Bull. (2022) 1–11.
[10] X. Shi, H. Xiao, H. Azarabadi, J. Song, X. Wu, X. Chen, K.S. Lackner, Sorbents for the direct capture of CO2 from ambient air, Angew. Chem. Int. Ed. 59 (18) (2020) 6984–7006.
[11] O. Shekhah, Y. Belmabkhout, Z. Chen, V. Guillerm, A. Cairns, K. Adil, M. Eddaoudi, Made-to-order metal-organic frameworks for trace carbon dioxide removal and air capture, Nat. Commun. 5 (1) (2014) 1–7.
[12] D.G. Madden, H.S. Scott, A. Kumar, K.-J. Chen, R. Sanii, A. Bajpai, M. Lusi, T. Curtin, J.J. Perry, M.J. Zaworotko, Flue-gas and direct-air capture of CO2 by porous metal–organic materials, Philosophical Transactions of the Royal Society A: Mathematical, Phys. Eng. Sci. 375 (2084) (2017) 20160025.
[13] A. Kumar, D.G. Madden, M. Lusi, K.J. Chen, E.A. Daniels, T. Curtin, J.J. Perry IV, M.J. Zaworotko, Direct air capture of CO2 by physisorbent materials, Angew. Chem. Int. Ed. 54 (48) (2015) 14372–14377.
[14] P.M. Bhatt, Y. Belmabkhout, A. Cadiau, K. Adil, O. Shekhah, A. Shkurenko, L. J. Barbour, M. Eddaoudi, A fine-tuned fluorinated MOF addresses the needs for trace CO2 removal and air capture using physisorption, J. Am. Chem. Soc. 138 (29) (2016) 9301–9307.
[15] V. Nikulshina, M. Gálvez, A. Steinfeld, Kinetic analysis of the carbonation reactions for the capture of CO2 from air via the Ca (OH) 2–CaCO3–CaO solar thermochemical cycle, Chem. Eng. J. 129 (1–3) (2007) 75–83.
[16] V. Nikulshina, C. Gebald, A. Steinfeld, CO2 capture from atmospheric air via consecutive CaO-carbonation and CaCO3-calcination cycles in a fluidized-bed solar reactor, Chem. Eng. J. 146 (2) (2009) 244–248.
[17] N. Masoud, G. Bordanaba-Florit, T. Van Haasterecht, J.H. Bitter, Effect of Support Surface Properties on CO2 Capture from Air by Carbon-Supported Potassium Carbonate, Ind. Eng. Chem. Res. 60 (38) (2021) 13749–13755.
[18] H.-X. Zhao, J.-C. Li, Y. Wang, Y.-R. Guo, S. Li, Q.-J. Pan, An environment-friendly technique for direct air capture of carbon dioxide via a designed cellulose and calcium system, Sep. Purif. Technol. 307 (2023), 122774.
[19] S. Wu, T. Beum, J. Yang, J. Kim, Properties of Ca-base CO2 sorbent using Ca (OH) 2 as precursor, Ind. Eng. Chem. Res. 46 (24) (2007) 7896–7899.
[20] P.-Q. Liao, X.-W. Chen, S.-Y. Liu, X.-Y. Li, Y.-T. Xu, M. Tang, Z. Rui, H. Ji, J.-P. Zhang, X.-M. Chen, Putting an ultrahigh concentration of amine groups into a metal–organic framework for CO 2 capture at low pressures, Chem. Sci. 7 (10) (2016) 6528–6533.
[21] J. Kothandaraman, A. Goeppert, M. Czaun, G.A. Olah, G.S. Prakash, Conversion of CO2 from air into methanol using a polyamine and a homogeneous ruthenium catalyst, J. Am. Chem. Soc. 138 (3) (2016) 778–781.
[22] F. Barzagli, M. Peruzzini, R. Zhang, Direct CO2 capture from air with aqueous and nonaqueous diamine solutions: a comparative investigation based on 13C NMR analysis, Carbon Capt. Sci. Technol. 3 (2022), 100049.
[23] Y. Wang, J.-T. Anyanwu, Z. Hu, R.T. Yang, Significantly enhancing CO2 adsorption on Amine-Grafted SBA-15 by boron doping and acid treatment for direct air capture, Sep. Purif. Technol. 309 (2023), 123030.
[24] N.J. Williams, C.A. Seipp, F.M. Brethomé, Y.-Z. Ma, A.S. Ivanov, V.S. Bryantsev, M. K. Kidder, H.J. Martin, E. Holguin, K.A. Garrabrant, CO2 capture via crystalline hydrogen-bonded bicarbonate dimers, Chem 5 (3) (2019) 719–730.
[25] R. Custelcean, Direct air capture of CO 2 via crystal engineering, Chem. Sci. 12 (38) (2021) 12518–12528.
[26] F.M. Brethomé, N.J. Williams, C.A. Seipp, M.K. Kidder, R. Custelcean, Direct air capture of CO2 via aqueous-phase absorption and crystalline-phase release using concentrated solar power, Nat. Energy 3 (7) (2018) 553–559.
[27] A. Kasturi, G.G. Jang, D. Stamberga, R. Custelcean, S. Yiacoumi, C. Tsouris, Determination of the regeneration energy of direct air capture solvents/sorbents using calorimetric methods, Sep. Purif. Technol. 310 (2023), 123154.
[28] S. Voskian, T.A. Hatton, Faradaic electro-swing reactive adsorption for CO 2 capture, Energ. Environ. Sci. 12 (12) (2019) 3530–3547.
[29] J.H. Rheinhardt, P. Singh, P. Tarakeshwar, D.A. Buttry, Electrochemical capture and release of carbon dioxide, ACS Energy Lett. 2 (2) (2017) 454–461.
[30] P. Singh, J.H. Rheinhardt, J.Z. Olson, P. Tarakeshwar, V. Mujica, D.A. Buttry, Electrochemical capture and release of carbon dioxide using a disulfide–thiocarbonate redox cycle, J. Am. Chem. Soc. 139 (3) (2017) 1033–1036.
[31] Q. Shu, M. Haug, M. Tedesco, P. Kuntke, H.V. Hamelers, Direct Air Capture Using Electrochemically Regenerated Anion Exchange Resins, Environ. Sci. Tech. (2022).
[32] T. Wang, K.S. Lackner, A. Wright, Moisture swing sorbent for carbon dioxide capture from ambient air, Environ. Sci. Tech. 45 (15) (2011) 6670–6675.
[33] X. Shi, H. Xiao, K.S. Lackner, X. Chen, Capture CO2 from Ambient Air Using Nanoconfined Ion Hydration, Angew. Chem. Int. Ed. 128 (12) (2016) 4094–4097.

[34] X. Shi, H. Xiao, K. Kanamori, A. Yonezu, K.S. Lackner, X. Chen, Moisture-driven CO2 sorbents, Joule 4 (8) (2020) 1823–1837.
[35] X. Wang, J. Song, Y. Chen, H. Xiao, X. Shi, Y. Liu, L. Zhu, Y.-L. He, X. Chen, CO2 absorption over ion exchange resins: the effect of amine functional groups and microporous structures, Ind. Eng. Chem. Res. 59 (38) (2020) 16507–16515.
[36] J. Song, L. Zhu, X. Shi, Y. Liu, H. Xiao, X. Chen, Moisture swing ion-exchange resin-PO4 sorbent for reversible CO2 capture from ambient air, Energy Fuel 33 (7) (2019) 6562–6567.
[37] T. Wang, J. Liu, H. Huang, M. Fang, Z. Luo, Preparation and kinetics of a heterogeneous sorbent for CO2 capture from the atmosphere, Chem. Eng. J. 284 (2016) 679–686.
[38] C. Hou, Y. Wu, T. Wang, X. Wang, X. Gao, Preparation of quaternized bamboo cellulose and its implication in direct air capture of CO2, Energy Fuel 33 (3) (2018) 1745–1752.
[39] J. Song, J. Liu, W. Zhao, Y. Chen, H. Xiao, X. Shi, Y. Liu, X. Chen, Quaternized chitosan/PVA aerogels for reversible CO2 capture from ambient air, Ind. Eng. Chem. Res. 57 (14) (2018) 4941–4948.
[40] C. Hou, D.R. Kumar, Y. Jin, Y. Wu, J.J. Lee, C.W. Jones, T. Wang, Porosity and hydrophilicity modulated quaternary ammonium-based sorbents for CO2 capture, Chem. Eng. J. 413 (2021), 127532.
[41] H. He, W. Li, M. Zhong, D. Konkolewicz, D. Wu, K. Yaccato, T. Rappold, G. Sugar, N.E. David, K. Matyjaszewski, Reversible CO 2 capture with porous polymers using the humidity swing, Energ. Environ. Sci. 6 (2) (2013) 488–493.
[42] H. He, M. Zhong, D. Konkolewicz, K. Yacatto, T. Rappold, G. Sugar, N.E. David, K. Matyjaszewski, Carbon black functionalized with hyperbranched polymers: synthesis, characterization, and application in reversible CO 2 capture, J. Mater. Chem. A 1 (23) (2013) 6810–6821.
[43] H. He, M. Zhong, D. Konkolewicz, K. Yacatto, T. Rappold, G. Sugar, N.E. David, J. Gelb, N. Kotwal, A. Merkle, Three-Dimensionally Ordered Macroporous Polymeric Materials by Colloidal Crystal Templating for Reversible CO2 Capture, Adv. Funct. Mater. 23 (37) (2013) 4720–4728.
[44] H. He, W. Li, M. Lamson, M. Zhong, D. Konkolewicz, C.M. Hui, K. Yaccato, T. Rappold, G. Sugar, N.E. David, Porous polymers prepared via high internal phase emulsion polymerization for reversible CO2 capture, Polymer 55 (1) (2014) 385–394.
[45] T. Wang, X. Wang, C. Hou, J. Liu, Quaternary functionalized mesoporous adsorbents for ultra-high kinetics of CO2 capture from air, Sci. Rep. 10 (1) (2020) 1–8.
[46] P. Forns, F. Albericio, Merrifield Resin, Encyclopedia of Reagents for Organic Synthesis (2001).
[47] M. Matsuda, K. Funabashi, T. Nishi, H. Yusa, M. Kikuchi, Decomposition of ion exchange resins by pyrolysis, Nucl. Technol. 75 (2) (1986) 187–192.
[48] J.T. Amphlett, M.D. Ogden, R.I. Foster, N. Syna, K. Soldenhoff, C.A. Sharrad, Polyamine functionalised ion exchange resins: Synthesis, characterisation and uranyl uptake, Chem. Eng. J. 334 (2018) 1361–1370.
[49] A. Traboulsi, N. Dupuy, C. Rebufa, M. Sergent, V. Labed, Investigation of gamma radiation effect on the anion exchange resin Amberlite IRA-400 in hydroxide form by Fourier transformed infrared and 13C nuclear magnetic resonance spectroscopies, Anal. Chim. Acta 717 (2012) 110–121.
[50] A.A. Zagorodni, D.L. Kotova, V.F. Selemenev, Infrared spectroscopy of ion exchange resins: chemical deterioration of the resins, React. Funct. Polym. 53 (2–3) (2002) 157–171.
[51] Z.S. Nickolov, O. Ozcan, J. Miller, FTIR analysis of water structure and its significance in the flotation of sodium carbonate and sodium bicarbonate salts, Colloids Surf A Physicochem Eng Asp 224 (1–3) (2003) 231–239.
[52] S. Choi, J.H. Drese, P.M. Eisenberger, C.W. Jones, Application of amine-tethered solid sorbents for direct CO2 capture from the ambient air, Environ. Sci. Tech. 45 (6) (2011) 2420–2427.
[53] M. Armstrong, X. Shi, B. Shan, K. Lackner, B. Mu, Rapid CO2 capture from ambient air by sorbent-containing porous electrospun fibers made with the solvothermal polymer additive removal technique, AIChE J 65 (1) (2019) 214–220.
[54] X. Sun, L. Zhu, P. Wang, W. Zhao, X. Chen, CO2 removal from natural gas by moisture swing adsorption, Chem. Eng. Res. Des. 176 (2021) 162–168.